Crystallography Reports, Vol. 43, No. 4, 1998, pp. 589–597. Translated from Kristallografiya, Vol. 43, No. 4, 1998, pp. 637–645.

Crystal Structure of $Na(Ca,Sr)_2Si_4O_{10}F$ Strontium Agrellite from Yakutian Charoitites: Agrellite Polytypes

I. V. Rozhdestvenskaya and L. V. Nikishova

St. Petersburg State University, Universitetskaya nab. 7/9, St. Petersburg, 199034 Russia

Received October 10, 1996; in final form, February 11, 1997

Abstract—The crystal structure of the natural mineral agrellite $Na(Ca,Sr)_2Si_4O_{10}F$ belonging to the family of charoitites (Yakutia) is refined. The structure is built up of alternating layers of the Ca cations and the Si_8O_{20} silicate "tunnels." The building layers are aligned parallel to the (010) plane and linked together by the Na atoms located in eight-membered rings of the tunnels. A comparison between structures of the studied mineral and rare-earth-containing agrellite (Canada) revealed some difference in relative positions of the silicate tunnel layers along the *b*-axis. Such positional difference is treated as a manifestation of the polytypism in this mineral group. The Canadian and Yakutian minerals are referred to, respectively, as agrellite-$2A_c$ and agrellite-$2A_I$.

INTRODUCTION

Our recent X-ray investigations on alkali calcium silicates (tokkoite, tinaksite, and canasites) from charoite rocks of the unique deposit Sirenevyi Kamen' (Murunskii massif, Yakutia) have revealed that calcium and sodium atoms making up octahedral slabs (layers) exhibit different distributions over the cation sites [1, 2]. It was shown that the general structural fragments in the minerals crystallizing in the course of metasomatic processes remained intact. In this work, we refined the crystal structure of the Murunskii strontium agrellite, which was kindly provided by K.A. Lazebnik (Yakutian Institute of Geological Sciences). The first comprehensive data (thermal gravimetric and X-ray diffraction analyses, IR spectroscopy, etc.) on strontium agrellite from fenites (Murunskii massif, Yakutia) were reported by Konev *et al.* [3]. The crystal structure of the rare-earth mineral $Na(Ca,RE)_2Si_4O_{10}F$ (Quebec, Canada) containing a small amount of rare-earth elements (*RE*) was thoroughly examined by Ghose and Wan [4]. In the crystal lattice of this mineral, layers of calcium polyhedra alternate with sodium silicate layers along the *b*-axis. The latter layers are formed by the $(Si_8O_{20})^{8-}$ silicate tunnel ribbons and the Na atoms located in the eight-membered rings of the tunnels. With allowance of the layered structure of agrellite, the authors of [4] assigned this mineral to a group of tunnel ribbon structures such as narsarsukite, lithidionite, fenaksite, canasite, and miserite [5]. Apart from some structural characteristics of the Canadian rare-earth agrellite, the Murunskii strontium agrellite $Na(Ca,Sr)_2Si_4O_{10}F$ exhibits special features that will be discussed below.

EXPERIMENTAL

A single-crystal X-ray investigation of charoitite minerals is complicated by a low quality of crystals that possess a perfect cleavage and undergo microtwining. A crystal $0.01 \times 0.05 \times 0.15$ mm in size was chosen for X-ray structure study. A set of experimental data was obtained on a $P2_1$ automated single-crystal diffractometer (MoK_α radiation; ω scan mode; scan speed, 2–30 deg/min) and included 722 reflections with $I > 2\sigma_I$), which is considerably less than the number of reflections used in the refinement of rare-earth agrellite (Table 1).

The mean values of the normalized structure amplitudes $|\bar{E}_{exp}|$ and $|\overline{E^2 - 1}|_{exp}$ are equal to 0.803 and 0.947, respectively; that is, they correspond to centrosymmetric (0.798 and 0.968) rather than noncentrosymmetric (0.886 and 0.736) structures. The centrosymmetric structure of the studied mineral was confirmed by the refinement. Our attempts to refine the structural parameters by using the atomic coordinates taken from [4] were unsuccessful. Hence, the structure was solved and refined independently by conventional X-ray diffraction analyses with the CSD software package [6]. The site occupancies for the octahedral and alkali cation sites were refined using 406 reflections with $\sin\theta/\lambda < 0.45$. The atomic coordinates and isotropic thermal parameters were refined from 616 reflections with $\sin\theta/\lambda > 0.1$ and $|F_{exp}| > 25$. Owing to a small number of reflections and a pseudocentering of the structure, the atoms in the sites related by pseudocentering were refined individually. After each refinement stage, the structure amplitudes were corrected for absorption according to the DIFABS program [7]. The final R_{iso} value was 0.062. With due regard for a small

1063-7745/98/4304-0589$15.00 © 1998 МАИК Наука/Interperiodica Publishing

Table 1. Crystal data for the $NaCa_2Si_4O_{10}F$ agrellites (space group $P\bar{1}$)

Parameter	Agrellite-Sr (I)	Agrellite-*RE* (II)
Occurrence	Murunskii massif, Yakutia	Quebec, Canada
Crystal chemical formula	$(Na_{0.94}K_{0.03})(Ca_{1.75}Sr_{0.16})(Si_4O_{10})$ $[F_{0.78}(O, OH)_{0.22}]0.24H_2O$	$(Na_{1.01}K_{0.02})(Ca_{1.82}RE_{0.12}M_{0.04})$ $(Si_{3.90}Al_{0.01}O_{9.92})[F_{0.93}(OH)_{0.18}]$
Simplified formula	$Na(Ca_{1.75}Sr_{0.16})$ $Si_4O_{10}[F, (OH)]$	$Na(Ca_{1.86}RE_{0.12})$ $Si_4O_{10}[F, (OH)]$
a, Å	7.788(4)	7.759(2)
b, Å	18.941(2)	18.946(3)
c, Å	6.995(4)	6.986(1)
α, deg	90.17(9)	89.88(2)
β, deg	116.78(8)	116.65(2)
γ, deg	94.16(4)	94.32(2)
V, Å^3	918(3)	914.7(4)
Z	4	4
D_m, g/cm^3	2.837	2.902
D_o, g/cm^3	2.832	2.887
Sample size, mm^3	$0.01 \times 0.05 \times 0.15$	$d = 0.25$
μ, cm^{-1}	26.68	18.20
$2\theta_{max}$	60.0	60.0
$N(I > 2\sigma_I)$	722	5343
N_{calcd}	616	5343
R_{iso}	0.062	0.076
R_{uniso}	0.054	0.045

number of reflections and a large number of refined parameters, the ultimate refinement of the anisotropic thermal parameters was carried out only for the cations and a part of oxygen atoms ($R_{uniso} = 0.053$). The final positional and isotropic thermal parameters for the structure of agrellite-Sr (**I**) are listed in Table 2.[1]

STRUCTURE DESCRIPTION

Ghose and Wan [4] determined the crystal structure of the Canadian agrellite-*RE* $Na(Ca,RE)_2Si_4O_{10}F$ (**II**) by X-ray single-crystal diffraction. In this structure, the slabs (layers) of Ca polyhedra are aligned parallel to the (010) plane and linked together by the $[Si_8O_{20}]^{8-}$ silicate tunnels lying along the *c*-axis. For clarity, we used the polyhedral representation of structure **II** (Fig. 1), contrary to [4]. The eight-membered rings of tunnel ribbons involve the Na^+ ions, which bind the tunnels into the layers lying parallel to the (010) plane (Fig. 2). Each unit cell contains two layers of the Ca polyhedra and two sodium silicate layers. A characteristic feature of structure **II** is the occurrence of the pseudo-*C*-centering, which clearly manifests itself for the coordinates of all atoms except for fluorine. The relevant pairs of atoms (designated in [4] as *A* and *B*) form two symmetry-different, even if close in configuration, silicate tunnels *A* and *B*. The projection of the structure onto the (010) plane indicates a pseudohexagonal motif of silicate tunnel packing. Since the fluorine atoms disturb the *C*-centering of the unit cell, the Ca atoms form different-type coordination polyhedra, for example, octahedra and seven-vertex polyhedra. The pairs of the Ca polyhedra related by the *C*-centering are also denoted by *A* and *B*.

As in structure **II**, the centering of the unit cell in structure **I** is also broken by fluorine atoms alone, and the Ca atoms are arranged in such a way that they meet both the *C*- and *I*-centerings (Table 2). Agrellites of these two types differ substantially in arrangement of the silicate tunnels and the related alkali cations. In **II**, the relative positions of the *A* and *B* sodium silicate layers can be characterized by the vector equal to one-half the diagonal in the (001) plane (the *C*-centering), and in **I**, by the lattice vector equal to one-half the body diagonal of the unit cell (the *I*-centering). To put it differently, with the same arrangement of octahedral slabs and silicate tunnels *A* in these structures, the silicate tunnels *B* and the related alkali cations are translated by *c*/2. This is associated with some features of the atomic distribution over the cation sites in the Ca slabs and dif-

[1] The tabulated anisotropic thermal parameters are available from the authors.

ferences in edge lengths of the Ca polyhedra in the structures of these minerals.

Features of the Ca slabs. The Ca polyhedra are formed by the O(4), O(5), O(8), and O(10) terminal oxygen atoms of silicate tunnels and by the F atoms (Fig. 1). The cations in the Ca(2*A*) and Ca(1*B*) sites have an octahedral coordination. The edge-sharing octahedra alternate along the *c*-axis to form the chains. The cations in the Ca(1*A*) and Ca(2*B*) sites exhibit a sevenfold coordination, which corresponds to a combination of a hemioctahedron and a trigonal prism. The seven-vertex polyhedra are joined to each other by the trigonal prism bases to form the chains along the *c*-axis. The chains of the vertex- and edge-sharing octahedra and seven-vertex polyhedra give rise to the Ca slab aligned parallel to the (010) plane. Along the *c*-axis, the unit cell involves two polyhedra of each chain. The *A* and *B* silicate tunnels are attached to the side edges of these polyhedra, which are formed by the O(4), O(8) and O(5), O(10) oxygen atoms alternating along the *c*-axis (Fig. 1).

In structures **I** and **II**, the main impurity elements (Sr and *RE*) reside in the Ca(1*A*) polyhedron (Table 3). The other sites in the Ca slabs in **II** are only slightly occupied by rare-earth elements. In structure **I**, the Ca atoms enter the Ca(2*B*) sites, and the Ca(1*B*) and Ca(2*A*) sites are equally occupied by the Ca and Na atoms. The last two sites have an octahedral coordination with the mean Ca–O distances equal to 2.34 and 2.35 Å, respectively (Table 4). The mean Ca–O distances in the Ca(1*A*) and Ca(2*B*) seven-vertex polyhedra (2.51 and 2.48 Å) are substantially larger than those in the octahedra.

Silicate radical. The silicate tunnel can be treated as consisting of two chains, each being formed by the Si(1), Si(2), Si(3), and Si(4) four-membered tetrahedral rings with the same O(1), O(3), O(7), and O(9) vertices (Fig. 1). These rings are linked into the vlasovite chain through the O(6) vertex common to both rings (Fig. 3) and share the O(2) bridging oxygen with tetrahedra of the centrosymmetrically related ring of the second vlasovite chain. The O(4), O(5), O(8), and O(10) terminal oxygen atoms of the tetrahedra are involved in the coordination polyhedra of the Ca slab. The silicate tunnel thus formed have four-, six-, and eight-membered rings, which are clearly seen, respectively, in Figs. 3, 1, and 2.

As noted above, the Na^+ alkali cations are located in the eight-membered rings. A portion of these sites is only partially occupied (Table 3). The interatomic distances and angles in the tetrahedra and the Na polyhedra (Table 4) are close to those in structure **II**; their values are typical of layered silicates.

Features of conjunction between the Ca slabs and the Si radicals. The role of geometric factor. It is of interest to compare the lengths of the O(5)–O(10) calcium polyhedron edges adjacent to the four-membered ring and the lengths of the O(5)–O(10) edges

Table 2. Fractional atomic coordinates and equivalent thermal parameters ($Å^{-2}$) for the agrellite-Sr structure

Site	*x/a*	*y/b*	*z/c*	B^*_{eq}
Ca(1*A*)	0.0068(8)	0.2188(3)	0.0023(9)	1.6(2)
Ca(1*B*)	0.5392(10)	0.2842(4)	0.0231(13)	0.8(2)
Ca(2*A*)	0.4491(10)	0.7203(5)	0.4754(12)	0.86(14)
Ca(2*B*)	0.9988(12)	0.7847(5)	0.4942(13)	2.0(3)
Si(1*A*)	0.208(2)	0.9287(8)	0.375(2)	2.2(4)
Si(1*B*)	0.3073(12)	0.5660(5)	0.1560(13)	0.9(3)
Si(2*A*)	0.486(2)	0.8753(6)	0.215(2)	1.7(2)
Si(2*B*)	0.0233(14)	0.6181(5)	0.2932(14)	0.6(1)
Si(3*A*)	0.8342(13)	0.9107(5)	0.6671(14)	1.0(1)
Si(3*B*)	0.6755(14)	0.5921(5)	0.834(2)	1.6(3)
Si(4*A*)	0.4866(15)	0.8793(5)	0.7673(15)	1.5(3)
Si(4*B*)	0.0255(13)	0.6209(5)	0.7285(13)	1.5(3)
Na(*A*)	0.235(2)	0.0082(8)	0.868(2)	2.6(5)
Na(*B*)	0.261(2)	0.5035(10)	0.628(3)	2.7(6)
F(*A*)	0.756(3)	0.7607(13)	0.131(4)	4.0(10)
F(*B*)	0.214(3)	0.2438(9)	0.375(2)	1.1(6)
O(1*A*)	0.359(3)	0.9384(10)	0.619(3)	0.7(3)
O(1*B*)	0.181(3)	0.5693(12)	0.902(3)	2.4(8)
O(2*A*)	0.097(3)	0.0072(10)	0.293(3)	0.5(6)
O(2*B*)	0.403(3)	0.4960(13)	0.199(3)	2.2(8)
O(3*A*)	0.348(4)	0.9354(13)	0.228(4)	3.1(10)
O(3*B*)	0.162(2)	0.5647(9)	0.266(3)	0.8(6)
O(4*A*)	0.062(4)	0.865(2)	0.277(4)	0.9(8)
O(4*B*)	0.455(3)	0.6366(14)	0.225(4)	1.9(5)
O(5*A*)	0.386(3)	0.7961(12)	0.189(3)	0.9(4)
O(5*B*)	0.100(3)	0.6954(12)	0.314(3)	0.7(4)
O(6*A*)	0.510(3)	0.906(2)	0.009(3)	3.1(9)
O(6*B*)	0.000(3)	0.5888(10)	0.500(3)	1.1(7)
O(7*A*)	0.698(3)	0.8925(12)	0.412(3)	1.4(7)
O(7*B*)	0.821(3)	0.6018(11)	0.107(3)	1.9(8)
O(8*A*)	0.021(3)	0.8722(12)	0.761(4)	2.0(8)
O(8*B*)	0.496(3)	0.6376(11)	0.748(3)	1.0(7)
O(9*A*)	0.703(3)	0.8930(10)	0.793(3)	0.7(3)
O(9*B*)	0.814(5)	0.596(2)	0.713(5)	5.7(15)
O(10*A*)	0.406(4)	0.8020(12)	0.698(4)	1.6(9)
O(10*B*)	0.114(3)	0.7016(10)	0.785(3)	0.43(4)

* $B_{eq} = \frac{1}{3}[B_{11}\, a^{*2} a^2 + \ldots 2B_{23}\, b^* c^*\, b\, c \cos(\alpha)]$.

Table 3. Occupancy factors for the cation sites in the structures of strontium and rare-earth agrellites

Site	Occupancy	
	agrellite-Sr	agrellite-*RE*
Ca(1*A*)	0.70(2) Ca + 0.30(2) Sr	0.8534 Ca + 0.1466(6) *RE*
Ca(1*B*)	0.86(4) Ca + 0.14(4) Na	0.978 Ca + 0.022(2) *RE*
Ca(2*A*)	0.90(4) Ca + 0.10(4) Na	0.993 Ca + 0.007(2) *RE*
Ca(2*B*)	1.00 Ca	0.985 Ca + 0.015 (2) *RE*
Na(*A*)	1.03(3) Na	Na
Na(*B*)	0.86(3) Na	Na

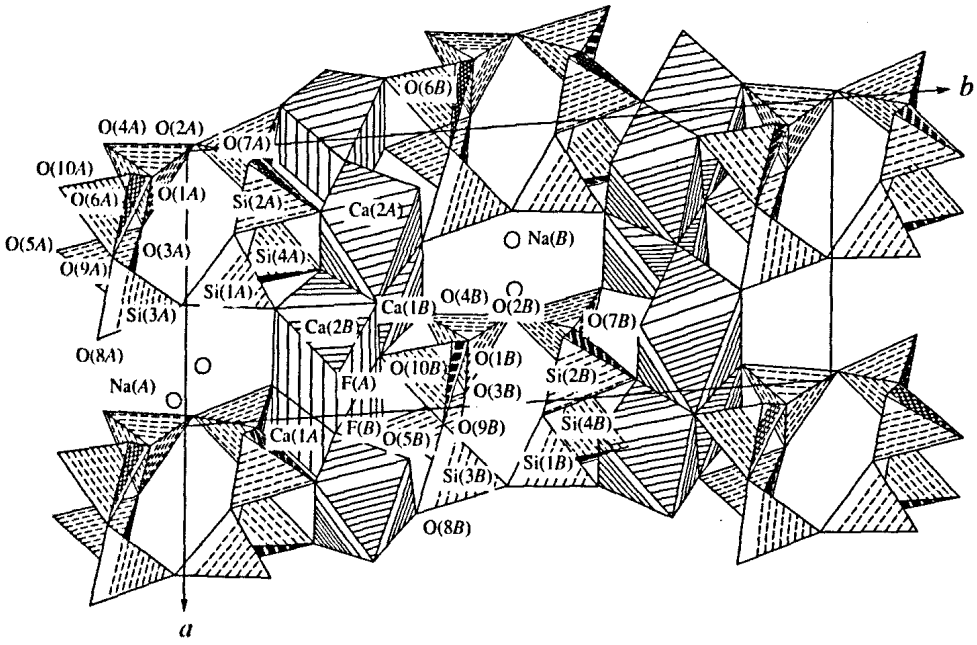

Fig. 1. Projection of the agrellite-Sr structure onto the *ab* plane.

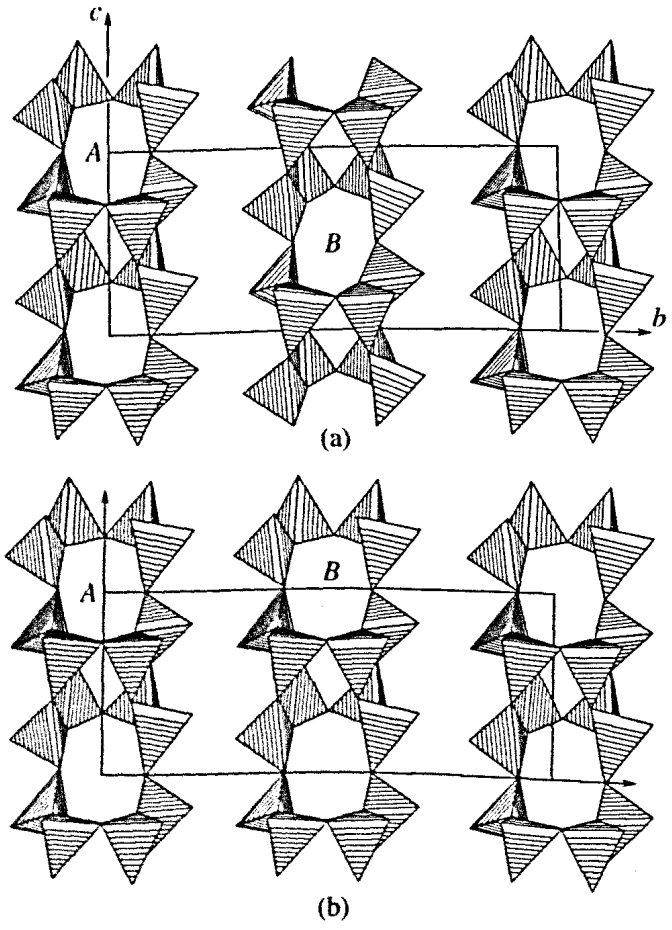

Fig. 2. Relative positions of the *A* and *B* silicate tunnels in (a) strontium and (b) rare-earth agrellite structures in projections onto the *bc* plane. The *B* tunnel in both structures is displaced by *a*/2 with respect to the *A* tunnel.

between the rings in the *A* and *B* tunnels in structures **I** and **II**. In both structures, the former edges turn out to be longer than the latter edges (Table 5). In structure **II**, the O(5*B*)–O(10*B*) edge of the Ca(1*A*) seven-vertex polyhedron with the highest content of rare-earth elements is the shortest (3.356 Å) and is located between the four-membered rings. In structure **I**, the O(5*A*)–O(10*A*) edge lengths of the Ca(2*A*) and Ca(1*B*) octahedra equally occupied by the Ca and Na atoms (Table 3) are close to each other (3.51 and 3.49 Å). The *A* silicate tunnel is adjacent to these edges. The four-membered ring of the *B* tunnel is attached to the longest O(5*B*)–O(10*B*) edge (3.75 Å) that belongs to the Ca(1*A*) seven-vertex polyhedron occupied by the Sr and Ca atoms.

Thus, the four-membered ring of the *A* tunnel in both structures is attached to the Ca(2*A*) octahedron edge (Fig. 1), whereas a similar ring of the *B* tunnel is attached to different polyhedra, specifically to the edge of the Ca(1*A*) seven-vertex polyhedron (structure **I**) and to the edge of the Ca(2*B*) seven-vertex polyhedron occupied predominantly by the Ca atoms (structure **II**) (Fig. 3). Such an attachment of the four-membered rings in the vlasovite chain to the longer edges of the Ca polyhedra provides an explanation for different relative positions of the *A* and *B* silicate radicals in the structures of strontium and rare-earth agrellites. Therefore, these two structures can be considered polytypes that differ in the positions of silicate radicals and whose formation is substantially affected by the geometric factor [the O(5)–O(10) edge lengths in the Ca polyhedra].

Table 4. Interatomic distances (Å) and angles (deg) for the agrellite-Sr structure

Si(1*A*)–O(1*A*)	1.67(2)	O(1*A*)–Si(1*A*)–O(2*A*)	104.6(15)
O(2*A*)	1.73(3)	O(1*A*)–Si(1*A*)–O(3*A*)	106.1(16)
O(3*A*)	1.70(3)	O(1*A*)–Si(1*A*)–O(4*A*)	118.8(18)
O(4*A*)	1.51(4)	O(2*A*)–Si(1*A*)–O(3*A*)	101.5(16)
	⟨1.65⟩	O(2*A*)–Si(1*A*)–O(4*A*)	111.8(18)
		O(3*A*)–Si(1*A*)–O(4*A*)	112.4(19)
			⟨109.2⟩
Si(1*B*)–O(1*B*)	1.60(2)	O(1*B*)–Si(1*B*)–O(2*B*)	107.3(16)
O(2*B*)	1.53(3)	O(1*B*)–Si(1*B*)–O(3*B*)	108.2(14)
O(3*B*)	1.62(2)	O(1*B*)–Si(1*B*)–O(4*B*)	105.1(15)
O(4*B*)	1.62(3)	O(2*B*)–Si(1*B*)–O(3*B*)	108.3(15)
	⟨1.59⟩	O(2*B*)–Si(1*B*)–O(4*B*)	115.0(16)
		O(3*B*)–Si(1*B*)–O(4*B*)	112.5(15)
			⟨109.4⟩
Si(2*A*)–O(3*A*)	1.65(4)	O(3*A*)–Si(2*A*)–O(5*A*)	111.9(16)
O(5*A*)	1.61(3)	O(3*A*)–Si(2*A*)–O(6*A*)	97.0(16)
O(6*A*)	1.64(3)	O(3*A*)–Si(2*A*)–O(7*A*)	107.3(16)
O(7*A*)	1.61(2)	O(5*A*)–Si(2*A*)–O(6*A*)	117.2(16)
	⟨1.63⟩	O(5*A*)–Si(2*A*)–O(7*A*)	117.8(15)
		O(6*A*)–Si(2*A*)–O(7*A*)	103.4(16)
			⟨109.1⟩
Si(2*B*)–O(3*B*)	1.61(3)	O(3*B*)–Si(2*B*)–O(5*B*)	112.7(15)
O(5*B*)	1.52(3)	O(3*B*)–Si(2*B*)–O(6*B*)	103.4(14)
O(6*B*)	1.63(2)	O(3*B*)–Si(2*B*)–O(7*B*)	107.6(14)
O(7*B*)	1.53(3)	O(5*B*)–Si(2*B*)–O(6*B*)	115.1(16)
	⟨1.57⟩	O(5*B*)–Si(2*B*)–O(7*B*)	113.9(16)
		O(6*B*)–Si(2*B*)–O(7*B*)	103.1(15)
			⟨109.2⟩
Si(3*A*)–O(2*A*)	1.59(3)	O(2*A*)–Si(3A)–O(7*A*)	110.2(14)
O(7*A*)	1.63(2)	O(2*A*)–Si(3*A*)–O(8*A*)	105.5(15)
O(8*A*)	1.54(3)	O(2*A*)–Si(3*A*)–O(9*A*)	107.4(14)
O(9*A*)	1.64(3)	O(7*A*)–Si(3*A*)–O(8*A*)	113.6(15)
	⟨1.60⟩	O(7*A*)–Si(3*A*)–O(9*A*)	107.8(14)
		O(8*A*)–Si(3*A*)–O(9*A*)	112.0(15)
			⟨109.4⟩
Si(3*B*)–O(2*B*)	1.71(3)	O(2*B*)–Si(3*B*)–O(7*B*)	102.5(14)
O(7*B*)	1.73(2)	O(2*B*)–Si(3*B*)–O(8*B*)	109.1(15)
O(8*B*)	1.58(3)	O(2*B*)–Si(3*B*)–O(9*B*)	102.0(17)
O(9*B*)	1.64(4)	O(7*B*)–Si(3*B*)–O(8*B*)	114.2(15)
	⟨1.66⟩	O(7*B*)–Si(3*B*)–O(9*B*)	108.5(17)
		O(8*B*)–Si(3*B*)–O(9*B*)	118.8(18)
			⟨109.2⟩
Si(4*A*)–O(1*A*)	1.60(3)	O(1*A*)–Si(4*A*)–O(6*A*)	100.7(15)
O(6*A*)	1.69(3)	O(1*A*)–Si(4*A*)–O(9*A*)	108.7(14)
O(9*A*)	1.61(3)	O(1*A*)–Si(4*A*)–O(10*A*)	116.0(16)
O(10*A*)	1.54(3)	O(6*A*)–Si(4*A*)–O(9*A*)	103.2(15)

Table 4. (Contd.)

	⟨1.61⟩	O(6*A*)–Si(4*A*)–O(10*A*)	115.4(17)
		O(9*A*)–Si(4*A*)–O(10*A*)	111.5(16)
			⟨109.2⟩
Si(4*B*)–O(1*B*)	1.66(3)	O(1*B*)–Si(4*B*)–O(6*B*)	102.2(14)
O(6*B*)	1.63(2)	O(1*B*)–Si(4*B*)–O(9*B*)	106.7(17)
O(9*B*)	1.63(4)	O(1*B*)–Si(4*B*)–O(10*B*)	109.0(14)
O(10*B*)	1.60(3)	O(6*B*)–Si(4*B*)–O(9*B*)	100.5(17)
	⟨1.63⟩	O(6*B*)–Si(4*B*)–O(10*B*)	115.2(14)
		O(9*B*)–Si(4*B*)–O(10*B*)	121.3(18)
			⟨109.0⟩
Si(1*A*)–O(1*A*)–Si(4*A*)	126.3(16)	Si(1*B*)–O(1*B*)–Si(4*B*)	138.3(18)
Si(1*A*)–O(2*A*)–Si(3*A*)	136.3(16)	Si(1*B*)–O(2*B*)–Si(3*B*)	135.6(19)
Si(1*A*)–O(3*A*)–Si(2*A*)	126.6(20)	Si(1*B*)–O(3*B*)–Si(2*B*)	136.7(15)
Si(2*A*)–O(6*A*)–Si(4*A*)	140.6(20)	Si(2*B*)–O(6*B*)–Si(4*B*)	137.3(17)
Si(2*A*)–O(7*A*)–Si(3*A*)	149.6(18)	Si(2*B*)–O(7*B*)–Si(3*B*)	148.4(18)
Si(3*A*)–O(9*A*)–Si(4*A*)	145.1(17)	Si(3*B*)–O(9*B*)–Si(4*B*)	147.0(26)
Ca(1*A*)–O(4*A*)	2.35(3)	Ca(1*B*)–F(*A*)	2.16(3)
F(*A*)	2.43(3)	O(8*B*)	2.29(3)
F(*B*)	2.43(2)	O(4*B*)	2.31(3)
O(8*A*)	2.46(3)	O(5*A*)	2.40(3)
O(5*B*)	2.60(3)	O(10*B*)	2.41(2)
O(10*B*)	2.61(3)	O(10*A*)	2.46(3)
O(5*A*)	2.72(3)		⟨2.34⟩
	⟨2.51⟩		
Ca(2*A*)–F(*B*)	2.21(2)	Ca(2*B*)–O(4*A*)	2.33(3)
O(10*A*)	2.34(3)	F(*A*)	2.40(3)
O(5*A*)	2.36(3)	O(8*A*)	2.43(3)
O(4*B*)	2.38(3)	O(10*B*)	2.45(3)
O(8*B*)	2.39(3)	F(*B*)	2.45(2)
O(5*B*)	2.43(3)	O(5*B*)	2.48(3)
	⟨2.35⟩	O(10*A*)	2.82(3)
			⟨2.48⟩
Na(*A*)–O(2*A*)	2.30(3)	Na(*B*)–O(2*B*)	2.33(3)
O(6*A*)	2.52(4)	O(6*B*)	2.41(3)
O(3*A*)	2.53(3)	O(6*B*)	2.53(3)
O(1*A*)	2.58(3)	O(3*B*)	2.60(3)
O(8*A*)	2.60(3)	O(1*B*)	2.61(3)
O(6*A*)	2.61(4)	O(9*B*)	2.85(4)
	⟨2.52⟩		⟨2.52⟩

AGRELLITE POLYTYPES

The choice of cells in the structures with the $(Si_8O_{20})^{8-}$ tunnel radical and the description of agrellite polytypes. Figure 4a schematically represents the structures with the $(Si_8O_{20})^{8-}$ tunnel radicals. The pseudohexagonal motif of the tunnel packing is clearly seen in the figure. If the atoms are equally distributed over the cation sites, the minimum structural fragment (the lattice parameters a_{min} and b_{min}), which involves one silicate tunnel and two cation sites, can be chosen as the unit cell. In Fig. 4b, this fragment is shown by

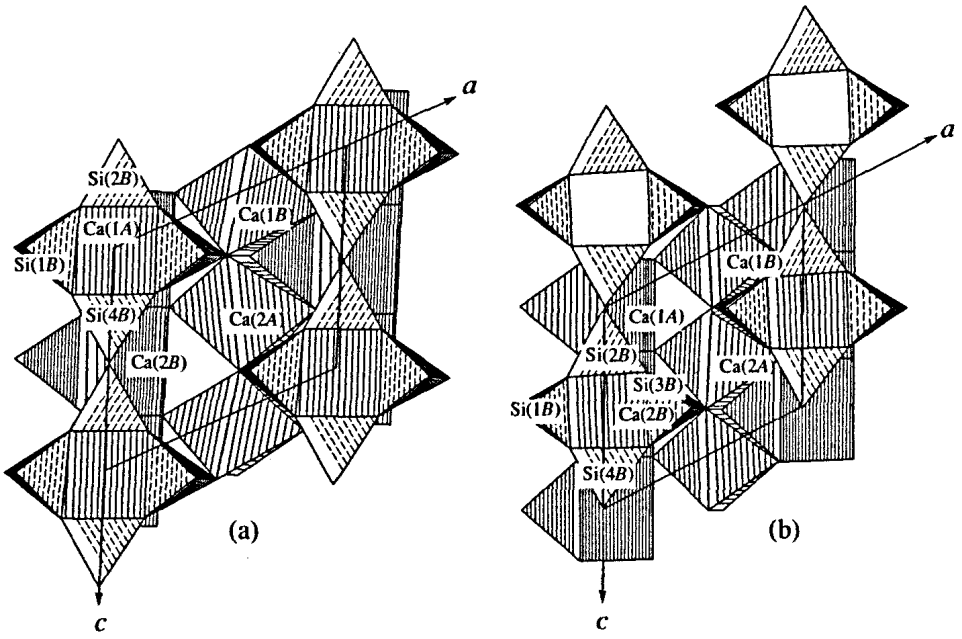

Fig. 3. Conjunction between the Ca slab located at a height of $z/c = 0.25$ and the vlasovite chain of the *B* silicate tunnel in (a) strontium and (b) rare-earth agrellite structures.

dashed lines. It is this fragment that is taken as the unit cell in the structures of the $K_2Na_2Cu_2(Si_8O_{20})$ lithidionite and $K_2Na_2Fe_2(Si_8O_{20})$ fenaksite (at different designations of axes) [5]. At the same time, the tunnels and the related Na^+ cations give rise to the puckered layers, which are aligned parallel to the (010) plane and alternate with the cation layers.

If the structural fragment that contains one layer of tunnel radicals (with alkali cations) and one cation layer is chosen as a building block, this structure can be treated as a hypothetical one-layer polytype with a triclinic unit cell, namely, $A(a_{min}b_{min}c)$ or $1A$ according to the Gard notation [8]. When the cations exhibit an ordering of the distribution over the sites, the unit cell is doubled (parameters: a_2, $b_2 = 2b_{min}$, c). This cell contains two tunnel and two cation layers (Fig. 4b, dotted line). However, from crystal chemical considerations, one can choose the pseudocentered triclinic unit cell with angles close to 90° (Fig. 4b, parameters: a, b, c), which does not affect the character of layer alternating.

In this case, structure **II** can be considered as a two-layer triclinic polytype with the pseudocentered *C* cell. The axes of the unit cell in structure **I** are identical to those in structure **II**. However, each second silicate layer is displaced by one-half the translation along the *c*-axis as compared to the location of a similar layer in structure **II**. Therefore, structure **I** can be treated as a two-layer triclinic polytype with the pseudocentered **I** cell. As mentioned above, the pseudocentering is caused by the fact that, in both structures, the fluorine atoms disturb the centering of the cells.

According to the recommendations given by Guinier *et al.* [8], these polytypes are described by the same modified Gard symbols: *Aabc*. However, with allowance made for the difference in the arrangement of the silicate layers, we referred to structures **I** and **II** as agrellite-$2A_I$ and agrellite-$2A_C$, respectively. Here, numeral 2 signifies a two-layer structure of polytype; letter *A* indicates triclinic symmetry; and subscripts *C* and *I* designate pseudo-*C*- and pseudo-*I*-centerings, respectively.

For a more correct description of the stacking sequence of layers, one can use the notion of modulated structures [9]. The building modules in the agrellite structure can be chosen in various ways. For example, these can be one-dimensional infinite silicate tunnels extended along the *c*-axis (Fig. 2) and two-dimensional calcium polyhedron layers parallel to the (010) plane (Fig. 3). In our case, it is expedient to choose larger structural modules—the two-dimensional puckered

Table 5. Lengths of the O(5)–O(10) edges (Å) in the Ca polyhedra of silicate radicals

Edge	Agrellite-Sr		Agrellite-*RE*	
	polyhedron	length	polyhedron	length
In four-membered ring				
O(5*A*)–O(10*A*)	Ca(2*A*)	3.51(3)	Ca(2*A*)	3.606(5)
O(5*B*)–O(10*B*)	Ca(1*A*)	3.75(3)	Ca(2*B*)	3.631(4)
Between four-membered rings				
O(5*A*)–O(10*A*)	Ca(1*B*)	3.49(3)	Ca(1*B*)	3.380(5)
O(5*B*)–O(10*B*)	Ca(2*B*)	3.25(3)	Ca(1*A*)	3.356(5)

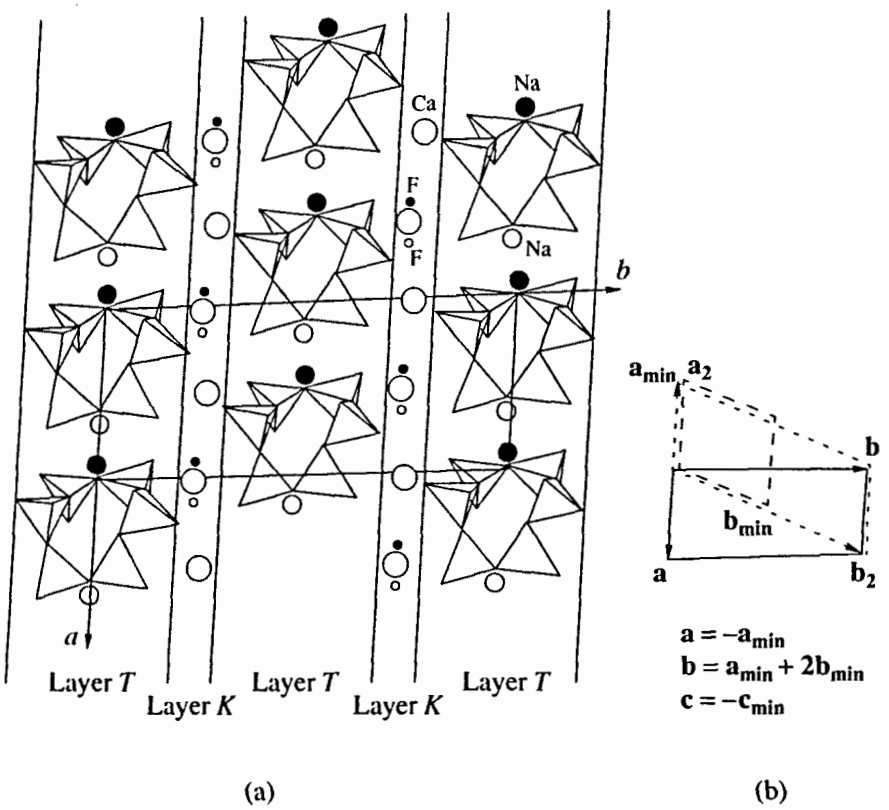

Fig. 4. (a) Schematic representation of the structures with tunnel radicals and (b) arrangement of axes in the minimum fragment and in doubled and pseudocentered unit cells in the agrellite structure. The filled and open circles correspond to the atomic sites located at heights of $+z$ and $-z$, respectively. The cross-section of the tunnel silicate radical is shown by tetrahedra.

sodium silicate layer *T* (Fig. 4a), which is aligned parallel to the (010) plane and involves the silicate tunnels with the related Na atoms; and the layer *K*, which includes the planes containing only Ca and F atoms, because all the oxygen atoms are involved in the silicon tetrahedra of the *T* layer. The successive *K* layers are related by the inversion centers located in the eight-membered tetrahedral rings in the silicate tunnels.

The stacking sequence of layers in the structure can be written as $|T_{pq}KT_{pq}K_{\bar{1}}|$, where *p* and *q* designate the only possible components of displacements of the *T* layers by ±1/2 along the *a*- and *c*-axes, respectively. Among all the possible combinations of "+" and "–" displacements, the structures of two-layer agrellite polytypes are characterized by two combinations given below.

Agrellite-*RE*(II)—$|T_{00}KT_{+0}K_{\bar{1}}|$ or |+0| in simplified form.

Agrellite-Sr—$|T_{00}KT_{++}K_{\bar{1}}|$ or |++| in simplified form.

The aforementioned structural features of the agrellite polytypes clearly manifest themselves in the X-ray powder diffraction patterns: the stronger reflections correspond to the pseudo-*C*-centering ($h + k = 2n$) for **II** and to the pseudo-*I*-centering ($h + k + l = 2n$) for **I** [10].

CONCLUSIONS

The structural data obtained for agrellite-Sr (**I**) and their comparison with those for agrellite-*RE* (**II**) make it possible to draw the following inferences:

(1) The ordering of strontium and rare-earth element atoms over particular cation sites in the agrellite structures brings about the doubling of the unit cell and the formation of two-layer agrellite polytypes.

(2) The centering of the *C* cell is associated with the pseudohexagonal motif of the silicate radical packing and the choice of the unit cell.

(3) The centering of the **I** cell in the agrellite-Sr structure is connected with the displacement of neighboring sodium silicate layers (*T*) by one-half the translation along the *c*-axis as compared to the arrangement of similar layers in the agrellite-*RE* structure. The position of the *B* tunnel in agrellite-Sr is determined by the geometric factor: the four-membered ring of the tunnel is attached to the longest edge of the polyhedron equally occupied by the Ca and Sr atoms.

(4) In both minerals, the F atoms break the centering of the cells, which thus become pseudocentered.

(5) In agrellite-Sr, the Na and Ca atoms are located in the octahedra. Moreover, the Na atoms also occupy the same sites in the eight-membered rings of tunnels that are occupied by the K atoms in many minerals with

tunnel radicals (canasite, miserite, franckamenite, and tinaksite).

ACKNOWLEDGMENTS

We would like to thank V.S. Fundamenskii for providing the CSD software package used in our calculations.

This work was supported by the Russian Foundation for Basic Research, project no. 96-05-65579.

REFERENCES

1. Rozhdestvenskaya, I.V., Nikishova, L.V., Lazebnik, Yu.D., and Lazebnik, K.A., *Z. Kristallogr.*, 1989, vol. 189, p. 195.
2. Nikishova, L.V., Lazebnik, K.A., Rozhdestvenskaya, I.V., Emel'yanova, N.N., and Lazebnik, Yu.D., *Mineral. Zh.*, 1992, no. 1, p. 71.
3. Konev, A.A., Vorob'ev, E.I., Sapozhnikova, A.N., *et al.*, *Mineral. Zh.*, 1987, no. 3, p. 73.
4. Ghose, S. and Wan, Ch., *Am. Mineral.*, 1979, vol. 64, nos. 5–6, p. 563.
5. *Mineraly: Spravochnik* (Minerals: A Handbook), Chukhrova, F.V., Ed., Moscow: Nauka, 1981, vol. 3, no. 3.
6. Akselrud, L.G., Grun, Yu.N., Zavalii, P.Yu., *et al.*, *Collect. Abstr. XII Eur. Crystallogr. Meet.*, Moscow, 1989, vol. 3, p. 155.
7. Walker, N. and Stuart, D., *Acta Crystallogr., Sect. A: Found. Crystallogr.*, 1983, vol. 39, no. 1, p. 158.
8. Guinier, A. *et al.*, *Acta Crystallogr., Sect. A: Found. Crystallogr.*, 1984, vol. 40, no. 4, p. 399.
9. Zvyagin, B.B., *Kristallografiya*, 1993, vol. 38, no. 1, p. 98.
10. Rozhdestvenskaya, I.V., Nikishova, L.V., and Lazebnik, K.A., *Zap. Vseross. Mineral. O–va*, 1998, part 77, no. 1, p. 89.

Translated by O. Borovik